Available online at www.sciencedirect.com
ScienceDirect
Comput. Methods Appl. Mech. Engrg. 279 (2014) 425–439
Computer methods in applied mechanics and engineering
www.elsevier.com/locate/cma

Isogeometric boundary-element analysis for the wave-resistance problem using T-splines

A.I. Ginnis[a,*], K.V. Kostas[b], C.G. Politis[b], P.D. Kaklis[a,c], K.A. Belibassakis[a], Th.P. Gerostathis[b], M.A. Scott[d], T.J.R. Hughes[e]

[a] School of Naval Architecture & Marine Engineering, National Technical University of Athens, Greece
[b] Department of Naval Architecture, Technological Educational Institute of Athens, Greece
[c] Department of Naval Architecture, Ocean and Marine Engineering, University of Strathclyde, United Kingdom
[d] Department of Civil and Environmental Engineering, Brigham Young University, United States
[e] Institute for Computational Engineering and Sciences, The University of Texas at Austin, United States

Received 31 January 2014; received in revised form 25 April 2014; accepted 2 July 2014
Available online 11 July 2014

Abstract

In this paper we couple collocated Boundary Element Methods (BEM) with unstructured analysis-suitable T-spline surfaces for solving a linear Boundary Integral Equation (BIE) arising in the context of a ship-hydrodynamic problem, namely the so-called Neumann–Kelvin problem, following the formulation by Brard (1972) and Baar and Price (1988). The local-refinement capabilities of the adopted T-spline bases, which are used for representing both the geometry of the hull and approximating the solution of the associated BIE, in accordance with the Isogeometric concept proposed by Hughes et al. (2005), lead to a solver that achieves the same error level for many fewer degrees of freedom as compared with the corresponding NURBS-based Isogeometric-BEM solver recently developed in Belibassakis et al. (2013). In this connection, this paper makes a step towards integrating modern CAD representations for ship-hulls with hydrodynamic solvers of improved accuracy and efficiency, which is a prerequisite for building efficient ship-hull optimizers.

Keywords: T-splines; Isogeometric analysis; BEM; Wave resistance

1. Introduction

Wave-making resistance is a very important component, which may contribute up to 50% – or even more – to the total resistance of a ship, especially for relatively "full" hull forms and/or at high speeds. Experience has shown that the wave-making resistance component is quite sensitive to changes to hull-form shape and significant reduction can be achieved without affecting cargo capacity. During the last 50 years, the interest in numerical methods for calculating ship wave resistance has been constantly growing. Computations are performed using a variety of techniques, ranging from the simple Michell's thin-ship theory [1] to extremely complex and costly methods such as the fully non-linear

* Corresponding author. Tel.: +30 2107723965.
E-mail addresses: ginnis@naval.ntua.gr (A.I. Ginnis), kvkostas@teiath.gr (K.V. Kostas), cpolitis@teiath.gr (C.G. Politis), kaklis@deslab.ntua.gr, panagiotis.kaklis@strath.ac.uk (P.D. Kaklis), kbel@fluid.mech.ntua.gr (K.A. Belibassakis), tgero@teiath.gr (Th.P. Gerostathis), michael.scott@byu.edu (M.A. Scott), hughes@ices.utexas.edu (T.J.R. Hughes).

http://dx.doi.org/10.1016/j.cma.2014.07.001
0045-7825/

Reynolds Averaged Navier Stokes Equations (RANSE) [2–4]; see the reports by the International Towing Tank Conference [5–7] and the references cited therein.

In all proposed methods a CAD model of the ship hull is required. However, analysis-suitable models cannot be, in general, automatically derived from CAD models. Data exchange between CAD and analysis methods requires many time-consuming, preparatory steps. For example, the popular meshing approach is generally time consuming and provides only an approximation of the exact CAD geometry. Furthermore, a recalculation of the generated mesh is required for even slight changes in the exact geometry. Thus, the lack of geometric exactness along with the, generally, cumbersome remeshing, render the requirements for rapid convergence and/or high precision prohibitive. These deficiencies in the current engineering analysis approach also preclude successful application of other procedures such as design optimization. In this case, the CAD-geometry-to-mesh mapping needs to be automatic and tightly integrated with the analysis solver and the optimizing environment. Enabling the automatic generation of geometrically exact and analysis suitable models could pave the way towards overcoming the aforementioned barriers. This aim can be achieved by appealing to IsoGeometric Analysis (IGA), introduced by Hughes et al. [8,9] and Cottrell et al. [10,11], which provides a direct and tight link between CAD and Computer Aided Engineering (CAE). This link is achieved by using the very same basis for representing both the geometry and the physical quantities employed in the analysis.

A number of candidate geometry representations can be used in the context of IGA. The geometrical representation, that is so far prevailing in CAD industry, is NURBS (Non-Uniform Rational B-Splines) [12]. NURBS representations offer: (1) convenience in modeling free-form parametric surfaces, (2) exact representation of all quadratic curves and surfaces that frequently occur in Mechanical-Engineering Design and (3) availability of many efficient and numerically-stable algorithms for their evaluation. NURBS also possess some mathematical properties that are useful from the analysis point of view: (a) refinability, such as the conventional h- (knot insertion) and p- (degree elevation) refinement schemes, as well as a more flexible refinement pattern, the so-called k-refinement, which is suitable for higher-order approximations, and (b) high smoothness, i.e., C^{p-1}-continuity for NURBS of degree $p \geq 2$, which prohibits derivative-jumps, thus, yielding more accurate results.

Isogeometric Analysis has been so far mainly applied in the FEM context, [10,9], where the basic preprocessing step is to develop good quality two- and three-dimensional (trivariate) representations of the computational domain. The latter is far from being a trivial problem and although different methods have been developed, e.g., lofting, swept-volume parameterization, Coons patches, etc., the literature is still lacking of a general and mature methodology. On the other hand, this approach differs from that adopted in contemporary CAD systems, namely the so-called Boundary Representation (B-Rep) of solids. In order to overcome these difficulties, a new approach for exploiting Isogeometric analysis has been presented. It is based on the boundary integral formulation of the problem considered, where the governing equations and the boundary conditions of the problem are transformed into a boundary integral equation (weakly singular or singular) on the boundary (or a portion of the boundary) using Green's function of the problem to be treated [13–19]. This approach is widely used in free-surface hydrodynamics, and especially in exterior potential-flow problems, due to the infinite extent of the fluid domain.

In the above context, our previous work [15], where a review of other pertinent works exploiting B-Spline/NURBS bases to discretize geometry or physical quantities or both can be found, has demonstrated the applicability and advantages of the Isogeometric approach to free-surface problems and especially to a linearized version of the wave-resistance problem, the so called "Neumann–Kelvin wave-resistance" problem, as initially proposed by Brard (1972) [20]. In this version of the problem, the potential flow theory is adopted and the non-linear effects stemming from the presence of the unknown free surface are neglected, while the three-dimensional character of the problem is retained. For the numerical solution of the resulting linear problem a Boundary-Element Method (BEM) was formulated, implemented by means of a Kelvin-wave source distribution over the wetted part of the hull and its intersection with the undisturbed free surface [21]. A multi-patch tensor product NURBS surface was used for the representation of the wetted ship hull boundary and the very same NURBS basis was used for the approximation of the unknown source density. The Isogeometric scheme was implemented by collocating at the images of the Greville abscissae of the associated knot vectors and knot insertion (h-refinement) is used as our refinement strategy. The enhanced accuracy and efficiency of the proposed NURBS based IsoGeometric Analysis BEM (IGA-BEM) has been demonstrated by comparing the numerical results obtained for a variety of geometrical configurations against analytical solutions and/or experimental data (where available) as well as predictions provided by low-order panel methods and higher-order BEMs. The tested configurations included a prolate spheroid in an infinite domain, a three-axial ellipsoid in

a semi-infinite domain, a submerged prolate spheroid under the free surface and three free-surface piercing hulls, namely the standard Wigley hull, a Series 60 and the so-called KRISO container ship hull [22].

However, the use of NURBS in Isogeometric Analysis exhibits some deficiencies:

1. Multi-patch representations suffer from gaps and overlaps at patch boundaries.
2. Due to their tensor-product nature a large number of NURBS control points are not unlikely to be superfluous, in the sense that they contain no significant geometric information. As a consequence, the resulting basis for approximating the physical quantities of interest, is "overloaded" with redundant detail in areas where these quantities are expected to exhibit low variation.
3. Refinement requires the insertion of entire rows/columns of control points, thus increasing complexity and implementation effort.
4. The limitations of rectangular topology lead to multi-patch representations when complex objects, as e.g., ship hulls, are under consideration. This limitation has an additional side-effect as multi-patch configurations can only secure a C^0 basis continuity across patch boundaries, canceling, in this way, the intrinsic higher smoothness of a single NURBS patch.

It is worth noticing that in the computer-aided ship-design literature one can already cite works arguing that NURBS do not offer the proper frame for ship design [23] and aspire to alternative representations [24]. These alternatives may include hierarchical splines [25], T-splines [26,27], PHT-splines (Polynomial Splines over Hierarchical T-meshes) [28] and LR-splines (Locally Refined splines) [29]. T-splines constitute a recently developed generalization of NURBS technology that removes most of the above mentioned NURBS deficiencies. The main advantages of T-splines technology are:

1. T-splines permit representation of complex objects with a single T-spline patch.
2. A T-spline control grid is allowed to have partial rows of control points, terminating in T-junctions, which allow for local refinement.
3. T-junctions permit the significant reduction of superfluous control points.
4. It is possible to merge multiple NURBS patches into a single, gap-free T-spline.

Our aim in the present work is to make a first step towards exploiting the advantages of T-splines technology in Isogeometric analysis (TS-IGA) for ship hydrodynamic analysis. The higher smoothness of a single T-spline surface along with the ability for local refinement allow us to achieve enhanced convergence rates with considerably fewer degrees of freedom when compared to our prior NURBS approach. This will permit our T-spline based IGA-BEM solver to be embedded with significantly lower cost in any optimization process for designing ship hulls with minimum wave resistance.

The remaining part of this paper is structured in 4 sections. Section 2 presents the formulation of the problem while Section 3 provides a brief overview of T-splines. We then proceed with the formulation of the problem in the Isogeometric T-spline BEM (TS-IGA-BEM) context and we conclude our work with two numerical examples demonstrating the achieved enhanced convergence: a prolate spheroid in infinite domain and a surface piercing ship hull.

2. Formulation of the problem

Let $Oxyz$ be a right-handed rectangular coordinate system with the z-axis directed vertically upwards; see Fig. 1. We consider the flow of a uniform stream with velocity $\mathbf{U} = (-U, 0, 0)$ of an ideal fluid with a free surface incident upon a surface piercing or fully submerged body D.

It is convenient to decompose the velocity potential Φ in the form:

$$\Phi = -Ux + \varphi, \tag{1}$$

where φ is the disturbance potential due to the presence of the submerged body. The disturbance potential must satisfy the Laplace equation (see, e.g., [21]):

$$\triangle\varphi = 0 \quad \text{in } D^+, \tag{2}$$

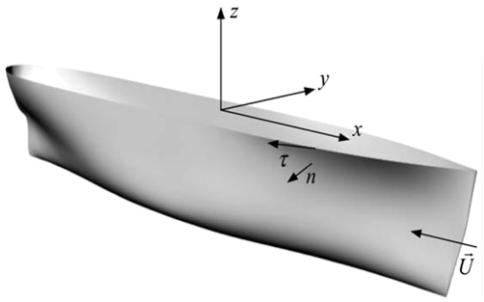

Fig. 1. Geometric configuration of the Neumann–Kelvin problem for a surface piercing body.

where D^+ denotes the unbounded fluid domain outside the body D limited above by the plane $z = 0$. The body boundary condition is

$$\frac{\partial \varphi}{\partial \mathbf{n}} = -\mathbf{U} \cdot \mathbf{n} \quad \text{on } S, \tag{3}$$

where $\mathbf{n} = (n_1, n_2, n_3)$ is the unit normal directed inwards with respect to the domain D^+ and $S = \partial D$ is the boundary of the body D. The free-surface conditions satisfied on the unknown free surface $z = \eta(x, y)$ are:

(i) The kinematic condition, stating that on the free surface the flow velocity must be tangential:

$$(-U + \varphi_x)\eta_x + \varphi_y \eta_y - \varphi_z = 0. \tag{4}$$

(ii) The dynamic condition, stating that the pressure on the free surface must be constant:

$$g\eta - U\varphi_x + \frac{1}{2}({\varphi_x}^2 + {\varphi_y}^2 + {\varphi_z}^2) = 0, \tag{5}$$

with g denoting the gravitational acceleration. In the theory of infinitesimal waves the above conditions on the free surface are linearized by neglecting products and squares of "small" quantities (stemming from the fact that the disturbance velocities are considered to be of higher order with respect to U) and by applying the resulting equations on the undisturbed free surface $z = 0$ instead of the unknown free surface $z = \eta(x, y)$. Thus, Eqs. (4) and (5) become, respectively,

$$U\eta_x + \varphi_z = 0, \tag{6}$$

$$g\eta - U\varphi_x = 0, \tag{7}$$

which can be combined to form the following linear free-surface condition:

$$\varphi_{xx} + k\varphi_z = 0 \quad \text{on } z = 0. \tag{8}$$

Here $k = g/U^2$ is the characteristic wavenumber, controlling the wavelength of the transverse ship waves and is proportional to the inverse square of the corresponding Froude number $F = U/\sqrt{gL}$, with L denoting the maximum length of the body.

Finally, a radiation condition must be imposed in order to ensure existence and uniqueness of the disturbance potential. This condition expresses that waves radiated by the body are directed downwards and there are no upstream waves. Mathematically, this condition is expressed as follows:

$$\varphi = \begin{cases} O\,(1/|x|) \\ o(1) \end{cases} \quad \text{as } |x| \to \infty, \quad \text{if } \begin{cases} x < 0 & \text{(downstream)}, \\ x > 0 & \text{(upstream)}. \end{cases} \tag{9}$$

Following the approach initiated by Brard (1972) [20] and explored in [21] for the linearized Neumann–Kelvin wave-resistance problem, the disturbance potential φ may be represented as

$$\varphi(\mathbf{P}) = \int_S \mu(\mathbf{Q}) G(\mathbf{P}, \mathbf{Q}) dS(\mathbf{Q}) + \frac{1}{k} \int_\ell \mu(\mathbf{Q}) G^*(\mathbf{P}, \mathbf{Q}) n_1(\mathbf{Q}) \tau_2(\mathbf{Q}) d\ell(\mathbf{Q}), \quad P \in D^+, \tag{10}$$

where μ is the density of the single-layer distribution on the wetted body boundary S and ℓ is the waterline of S, which exists only in the case of a surface piercing body. In the above equation $G(\mathbf{P}, \mathbf{Q})$ denotes the associated Green's function of the Neumann–Kelvin problem defined as:

$$4\pi G(\mathbf{P}, \mathbf{Q}) = r^{-1} - (r')^{-1} + G^*(\mathbf{P}, \mathbf{Q}), \quad \mathbf{Q} \in S,\ \mathbf{P} \in D^+ \cup S, \tag{11}$$

where $r = \|\mathbf{P}-\mathbf{Q}\|$, $r' = \|\mathbf{P}-\mathbf{Q}'\|$ with $\mathbf{Q}'$ denoting the image of $\mathbf{Q}$ with respect to the undisturbed free surface $z = 0$ and $G^*(\mathbf{P}, \mathbf{Q})$ stands for the regular part of Neumann–Kelvin Green's function, consisting of exponential decaying and wavelike components; for more details see Baar and Price (1988) [21]. Furthermore, $\boldsymbol{\tau} = (\tau_1, \tau_2, \tau_3)$ denotes the tangent vector along the waterline ℓ, directed as shown in Fig. 1.

The use of (11) enables automatic satisfaction of the linearized condition on the undisturbed free surface (Fig. 1) and the conditions at infinity. Using all the above, the Neumann–Kelvin problem is equivalently reformulated as a BIE on the body boundary S, characterized by a weakly singular kernel,

$$\frac{\mu(\mathbf{P})}{2} - \int_S \mu(\mathbf{Q}) \frac{\partial G(\mathbf{P}, \mathbf{Q})}{\partial n(\mathbf{P})} dS(\mathbf{Q}) - \frac{1}{k} \int_\ell \mu(\mathbf{Q}) \frac{\partial G^*(\mathbf{P}, \mathbf{Q})}{\partial n(\mathbf{P})} n_1(\mathbf{Q}) \tau_2(\mathbf{Q}) d\ell(\mathbf{Q}) = \mathbf{U} \cdot \mathbf{n}(\mathbf{P}), \quad \mathbf{P}, \mathbf{Q} \in S. \tag{12}$$

From the solution of the above integral equation, various quantities, such as velocity, pressure distribution and ship wave pattern can be obtained. Specifically, total flow velocity and pressure are readily obtained by

$$\mathbf{w} = \mathbf{U} + \nabla\varphi, \tag{13}$$

$$p = p_\infty + \frac{\rho}{2}(U^2 - \|\mathbf{w}\|^2) - \rho g z, \tag{14}$$

where ρ is the fluid density and p_∞ is the ambient pressure. The deviation of pressure p from p_∞ is measured via the non-dimensional pressure coefficient

$$C_p = \frac{p - p_\infty}{\frac{\rho}{2}U^2} = 1 - \frac{\|\mathbf{w}\|^2 + 2gz}{U^2}. \tag{15}$$

Finally, the free-surface elevation is obtained by

$$\eta(x, y) = (U/g) \cdot \varphi_x(x, y; z = 0). \tag{16}$$

We conclude this section by noting that in the case of a fully submerged body the above formulation should be modified by dropping the waterline integral in Eqs. (10) and (12).

3. T-splines: a brief introduction

In this section, we present a brief overview of T-spline technology. For additional details the interested reader is referred to Sederberg et al. (2003) [26,30], Sederberg et al. (2004) [31], Bazilevs et al. (2010) [27], Scott et al. (2011) [32] and Scott et al. (2012) [33]. In what follows we focus on cubic T-spline surfaces due to their predominance in industry. We denote the spatial and parametric dimensions by d_s and d_p, respectively. We denote an element index by e and the number of non-zero basis functions over an element e by n.

3.1. The unstructured T-mesh

An important object of interest underlying T-spline technology is the T-mesh. For surfaces, a T-mesh is a polygonal mesh and we will refer to the constituent polygons as elements or, equivalently, faces. Each element is a quadrilateral whose edges are permitted to contain T-junctions — vertices that are analogous to hanging nodes in finite elements. A control point, $\mathbf{P}_A \in \mathbb{R}^{d_s}, d_s = 2, 3$ and a control weight, $w_A \in \mathbb{R}$, where the index A denotes a global control point number, is assigned to every vertex in the T-mesh. The valence of a vertex is the number of edges that touch the vertex. An extraordinary point is an interior vertex that is not a T-junction and whose valence does not equal four.

Fig. 2 shows an unstructured T-mesh. Notice the valence three and valence five at extraordinary points denoted by hollow circles. The single T-junction is denoted by a hollow square.

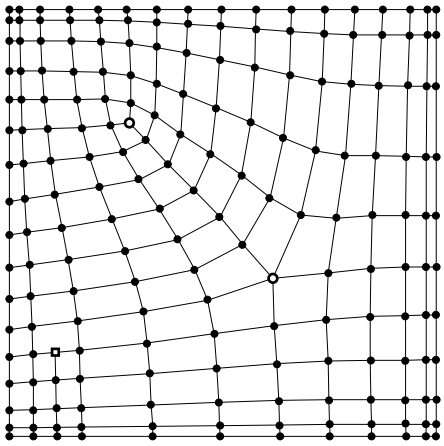

Fig. 2. An unstructured T-mesh. Extraordinary points are denoted by hollow circles and T-junctions are denoted by hollow squares.

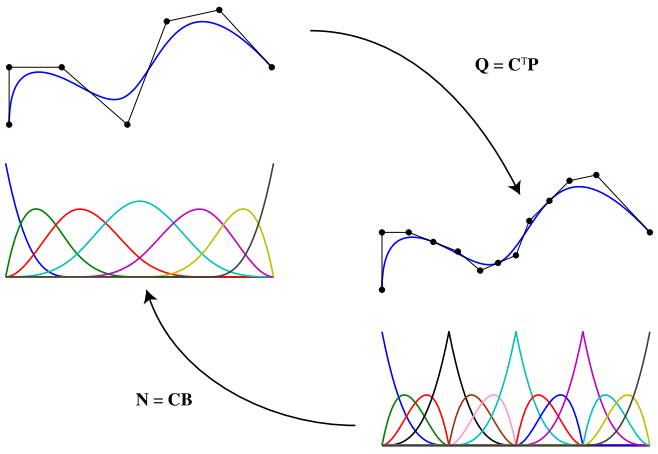

Fig. 3. Schematic representation of Bézier extraction for a B-spline curve. B-spline basis functions and control points are denoted by **N** and **P**, respectively. Bernstein polynomials and control points are denoted by **B** and **Q**, respectively. The curve $T(\boldsymbol{\xi}) = \mathbf{P}^T\mathbf{N}(\boldsymbol{\xi}) = \mathbf{Q}^T\mathbf{B}(\boldsymbol{\xi})$.

To define a basis, a valid knot interval configuration must be assigned to the T-mesh. A knot interval is a non-negative real number assigned to an edge. A valid knot interval configuration requires that the knot intervals on opposite sides of every element sum to the same value. In this paper, we require that the knot intervals for spoke edges of an individual extraordinary point either be all non-zero or all zero.

3.2. Bézier extraction

In this paper, we develop T-splines from the finite element point-of-view, utilizing Bézier extraction [34,32]. The idea is to extract the linear operator which maps the Bernstein polynomial basis on Bézier elements to the global T-spline basis. The linear transformation is defined by a matrix referred to as the extraction operator and denoted by $\mathbf{C}^e$. The transpose of the extraction operator maps the control points of the global T-spline to the control points of the Bernstein polynomials. Fig. 3 illustrates the idea for a B-spline curve. This provides a finite element representation of T-splines, and facilitates the incorporation of T-splines into existing finite element programs. Only the shape function subroutine needs to be modified. All other aspects of the finite element program remain the same. Additionally, Bézier extraction is automatic and can be applied to any T-spline regardless of topological complexity or polynomial degree. In particular, it represents an elegant treatment of T-junctions, referred to as hanging nodes in finite element analysis.

3.3. The T-spline basis

A T-spline basis function, N_A, is defined for every vertex, A, in the T-mesh. Each N_A is a bivariate piecewise polynomial function. If A is not adjacent to an extraordinary point, N_A is comprised of a 4×4 grid of polynomials. Otherwise, the polynomials comprising N_A do not form a 4×4 grid but rather an unstructured grid of polynomials. In either case, the polynomials can be represented in Bézier form. Because of this, Bézier extraction can be applied to an entire T-spline to generate a finite set of Bézier elements such that

$$\mathbf{N}^e(\tilde{\boldsymbol{\xi}}) = \mathbf{C}^e\mathbf{B}(\tilde{\boldsymbol{\xi}}), \tag{17}$$

where $\tilde{\boldsymbol{\xi}} \in \tilde{\Omega}$ is a coordinate in a standard Bézier parent element domain, $\mathbf{N}^e(\tilde{\boldsymbol{\xi}}) = \{N_a^e(\tilde{\boldsymbol{\xi}})\}_{a=1}^n$ is a vector of T-spline basis functions which are non-zero over Bézier element e, $\mathbf{B}(\tilde{\boldsymbol{\xi}}) = \{B_i(\tilde{\boldsymbol{\xi}})\}_{i=1}^m$ is a vector of tensor product Bernstein polynomial basis functions defining Bézier element e and $\mathbf{C}^e \in \mathbb{R}^{n\times m}$ is the element extraction operator.

3.4. The T-spline discretization

We can define the element geometric map, $\mathbf{X}^e : \tilde{\Omega} \rightarrow \Omega^e$, from the parent element domain onto the physical domain in the reference configuration as

$$\mathbf{X}^e(\tilde{\boldsymbol{\xi}}) = \frac{1}{(\mathbf{w}^e)^T\,\mathbf{N}^e(\tilde{\boldsymbol{\xi}})}\left(\mathbf{P}^e\right)^T\mathbf{W}^e\mathbf{N}^e(\tilde{\boldsymbol{\xi}}) \tag{18}$$

$$= \left(\mathbf{P}^e\right)^T\mathbf{R}^e(\tilde{\boldsymbol{\xi}}) \tag{19}$$

where $\mathbf{R}^e(\tilde{\boldsymbol{\xi}}) = \{R_a^e(\tilde{\boldsymbol{\xi}})\}_{a=1}^n$ is a vector of rational T-spline basis functions, the element weight vector $\mathbf{w}^e = \{w_a^e\}_{a=1}^n$, the diagonal weight matrix $\mathbf{W}^e = \mathrm{diag}(\mathbf{w}^e)$, and $\mathbf{P}^e$ is a matrix of dimension $n \times d_s$ that contains element control points,

$$\mathbf{P}^e = \begin{bmatrix} P_1^{e,1} & P_1^{e,2} & \dots & P_1^{e,d_s} \\ P_2^{e,1} & P_2^{e,2} & \dots & P_2^{e,d_s} \\ \vdots & \vdots & & \vdots \\ P_n^{e,1} & P_n^{e,2} & \dots & P_n^{e,d_s} \end{bmatrix}. \tag{20}$$

Using (18) and (19) we have that

$$\mathbf{R}^e(\tilde{\boldsymbol{\xi}}) = \frac{1}{(\mathbf{w}^e)^T\,\mathbf{N}^e(\tilde{\boldsymbol{\xi}})}\mathbf{W}^e\mathbf{N}^e(\tilde{\boldsymbol{\xi}}), \tag{21}$$

and using (17)

$$\mathbf{R}^e(\tilde{\boldsymbol{\xi}}) = \frac{1}{(\mathbf{w}^e)^T\,\mathbf{C}^e\mathbf{B}(\tilde{\boldsymbol{\xi}})}\mathbf{W}^e\mathbf{C}^e\mathbf{B}(\tilde{\boldsymbol{\xi}}). \tag{22}$$

Note that all quantities in (22) are written in terms of the Bernstein basis defined over the parent element domain, $\tilde{\Omega}$.

4. T-spline based isogeometric BEM

The Isogeometric Analysis philosophy attempts to define the approximate field quantities (dependent variables) of the boundary-value problem in question from the basis that is being used for representing the geometry of the body boundary. In the case of the boundary integral equation (12), the dependent variable is the source–sink density μ, distributed over the body boundary S. The latter is accurately and efficiently represented as a T-spline surface, as below:

$$S = \bigcup_{e=1}^{n_e} S_e, \qquad S_e(\tilde{\boldsymbol{\xi}}) = \sum_{i=1}^{n_{cp}} \mathbf{d}_i\,R_i^e(\tilde{\boldsymbol{\xi}}), \quad \tilde{\boldsymbol{\xi}} \in \tilde{\Omega}_e, \tag{23}$$

where n_{cp} is the number of control points, or T-mesh vertices, $\mathbf{d}_i$ in the T-mesh, R_i^e is the restriction of the rational T-spline basis function R_i at $\tilde{\Omega}_e$, and n_e is the number of elements. In conformity with the IGA concept, the unknown

source–sink surface distribution μ is approximated by the very same T-splines basis used for the body-boundary representation (23), that is:

$$\mu(\mathbf{P}) = \sum_{i=1}^{n_{cp}} \mu_i \tilde{R}_i(\mathbf{P}), \quad \mathbf{P} \in S, \tag{24}$$

where $\tilde{R}_i(\mathbf{P}) \equiv R_i^e(\tilde{\boldsymbol{\xi}}(\mathbf{P}))$, $\mathbf{P} \in S_e$. Inserting Eq. (24) into the BIE (12) we get:

$$\frac{1}{2}\sum_{i=1}^{n_{cp}} \mu_i \tilde{R}_i(\mathbf{P}) - \sum_{i=1}^{n_{cp}} \mu_i \mathbf{n}(\mathbf{P}) \cdot \mathbf{u}_i(\mathbf{P}) = \mathbf{U} \cdot \mathbf{n}(\mathbf{P}), \quad \mathbf{P} \in S, \tag{25}$$

where

$$\mathbf{u}_i(\mathbf{P}) = \int_S \tilde{R}_i(\mathbf{Q}) \nabla_P G(\mathbf{P}, \mathbf{Q}) dS(\mathbf{Q}) + k^{-1} \int_\ell \tilde{R}_i(\mathbf{Q}) \nabla_P G^*(\mathbf{P}, \mathbf{Q}) n_1(\mathbf{Q}) \tau_2(\mathbf{Q}) d\ell(\mathbf{Q}) \tag{26}$$

are the so-called induced velocity factors and $\nabla_A F(\mathbf{A}, \mathbf{B})$ denotes the gradient of F with respect to $\mathbf{A}$.

We now collocate Eq. (25) by specifying n_{cp} collocation points $\mathbf{P}_j$, $j = 1, \ldots, n_{cp}$, on S. For smooth ship hulls, these points are chosen to be the 1-ring collocation points for both the non-extraordinary and extraordinary vertices of the T-mesh, as defined in [18]. This definition of collocation points is a generalization of the Greville abscissae for the cases of unstructured grids, T-junctions and extraordinary points. However, when T-splines have no T-junctions or extraordinary points, the 1-ring collocation points described in [18] are equivalent to the two-dimensional Greville abscissae. In this way, we obtain the following linear system of equations with respect to the unknown coefficients μ_i:

$$\sum_{i=1}^{n_{cp}} \mu_i \left[\tilde{R}_i(\mathbf{P}_j) - 2\mathbf{n}(\mathbf{P}_j) \cdot \mathbf{u}_i(\mathbf{P}_j) \right] = 2\mathbf{U} \cdot \mathbf{n}(\mathbf{P}_j), \quad j = 1, \ldots, n_{cp}. \tag{27}$$

In the above equation, the integrals involved in the calculation of the induced velocity factors (Eq. (26)) are localized to integrals over Bézier elements using the Bézier extraction framework described in Section 3.2. Moreover, since these singular integrals are defined in the Cauchy Principal Value (CPV) sense, we employ the following technique for their accurate and robust numerical calculation: We exclude an ϵ-neighborhood, with $\epsilon \to 0$, around the singularity at the collocation point $\mathbf{P}_j$ and make sure that the size of integration's intervals, near the singularity, tend to 0 as $\epsilon \to 0$. More details on the treatment of the singular integrals and the achieved rates of convergence can be found in [15]. In order to maintain a uniform numerical scheme for the calculation of the CPV integrals, we need to make sure that the collocation point $\mathbf{P}_j$ lies inside a Bézier element (and not on an edge). If this is not the case, we shift appropriately the corresponding collocation point.

5. Numerical results and discussion

In order to test the efficiency and accuracy of the T-spline BEM methodology developed in the previous sections, we shall now present and discuss its performance in tests involving an ellipsoid (Section 5.1) and a ship hull (Section 5.2). Efficiency will be investigated by comparing locally-refined T-splines with non-locally refined NURBS. The error will be compared with either analytically available solutions or reference solutions provided by the NURBS solver after a dense global refinement.

5.1. A prolate spheroid in an infinite domain

In this example, we consider a prolate spheroid with axes $a, b = c$, and ratio $a : b = 5 : 1$, moving at constant speed $\mathbf{U} = (-U, 0, 0)$ in an infinite homogeneous fluid. In this case, an analytical expression of the velocity $\mathbf{w}$ on the surface of the ellipsoid is available, namely:

$$\mathbf{w}(\mathbf{P}) = \frac{2}{2 - a_0}\big(\mathbf{U} - U n_1(\mathbf{P})\mathbf{n}(\mathbf{P})\big), \tag{28}$$

$$a_0 = \frac{1 - \epsilon^2}{\epsilon^3}\left(-2\epsilon + \ln\left(\frac{1+\epsilon}{1-\epsilon}\right)\right), \quad \epsilon = \sqrt{1 - (b/a)^2}; \tag{29}$$

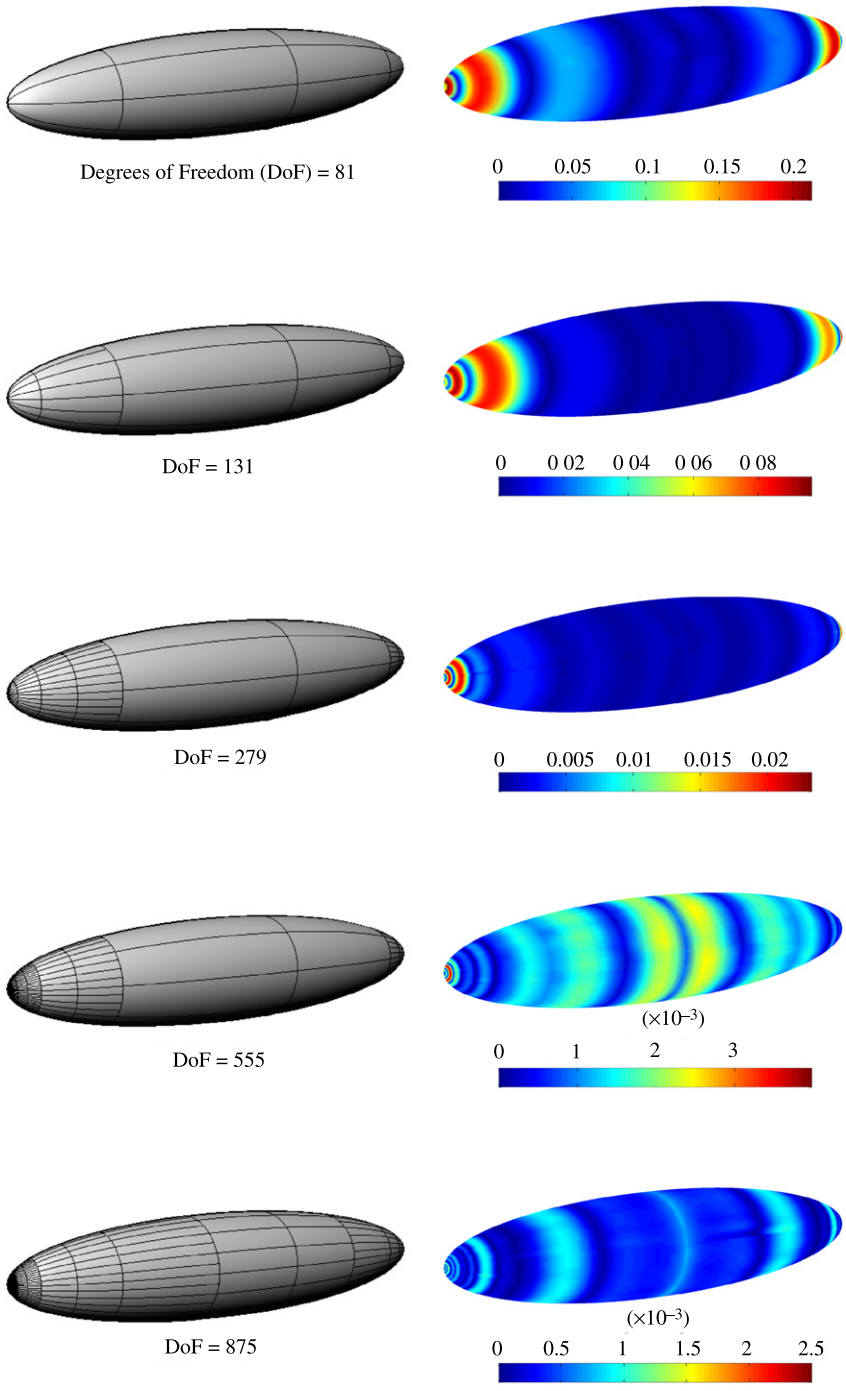

Fig. 4. T-spline refinement steps (left column) along with the corresponding velocity error distribution (right column).

(see e.g. [35,36]). In our study the L^2-error associated with the velocity field on the body surface is defined as follows:

$$\left\|\mathbf{w}-\mathbf{w}^{\mathbf{r}}\right\|_{L^2}=\left(\int_S\left\|\mathbf{w}(\mathbf{P})-\mathbf{w}^{\mathbf{r}}(\mathbf{P})\right\|^2 dS(\mathbf{P})\right)^{\frac{1}{2}} \tag{30}$$

where $\mathbf{w}^{\mathbf{r}}$ denotes the IGA-BEM approximation of $\mathbf{w}$ corresponding to the refinement level r. Fig. 4 depicts the T-mesh of the spheroid along with the corresponding pointwise error $\|\mathbf{w}(\mathbf{P})-\mathbf{w}^{\mathbf{r}}(\mathbf{P})\|$ of the velocity for five refinement steps.

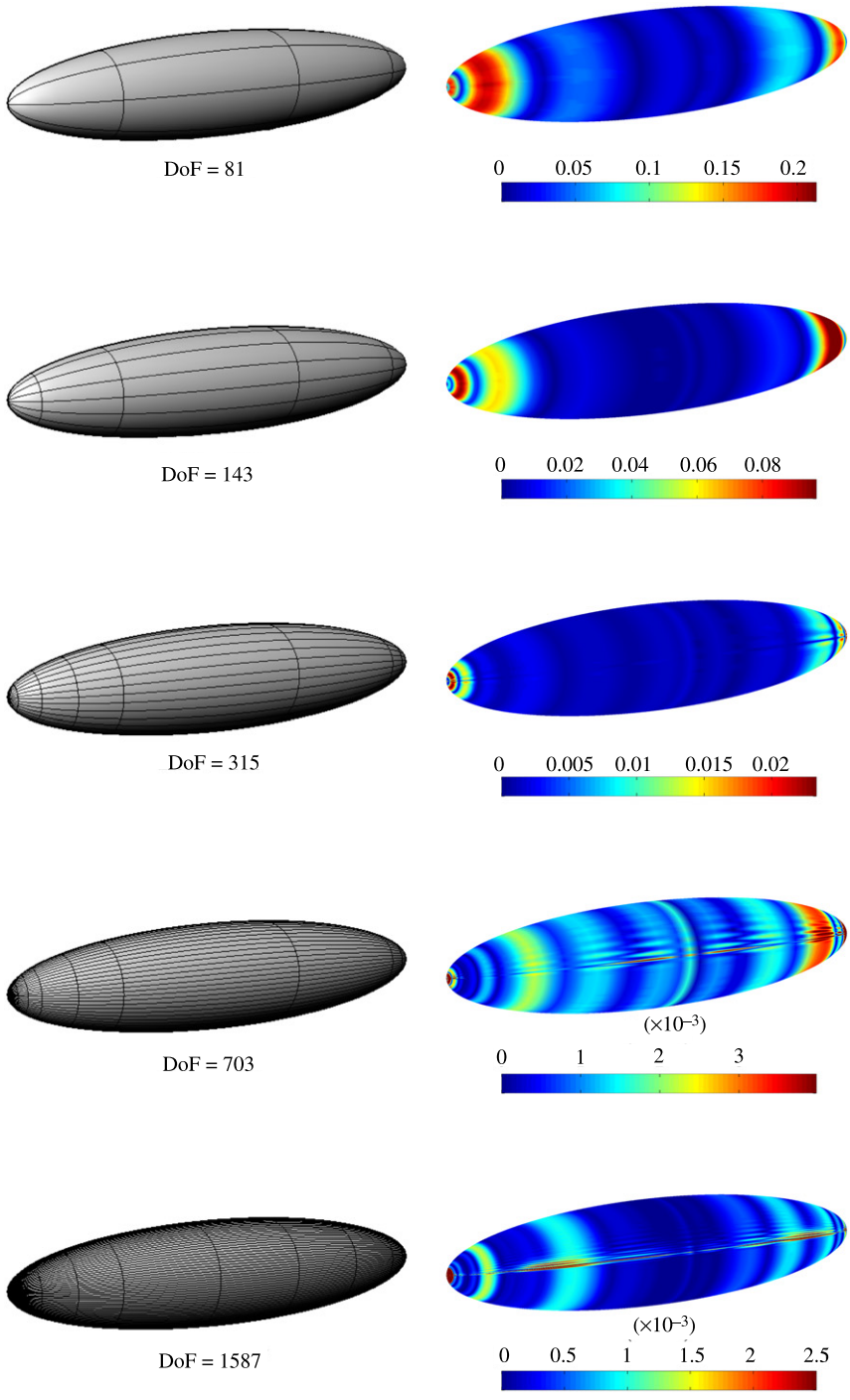

Fig. 5. NURBS refinement steps (left column) along with the corresponding velocity error distribution (right column).

Each refinement level r is obtained by locally h-refining the T-mesh at level $r-1$ in areas where the error is high. This manual refinement process manages to reduce the L^{∞}-error from 10^{-1} to 10^{-3}. The corresponding NURBS based process, where each T-mesh is replaced by its unique NURBS refinement, is given in Fig. 5. Note that the fluctuations exhibited in the error distribution for the last two refinements (DoF = 703,1587) is due to the extremely elongated elements in the area. A way to alleviate this behavior would be to refine the other parametric direction as well. However, in this case, the NURBS representation would not correspond to the T-Spline one.

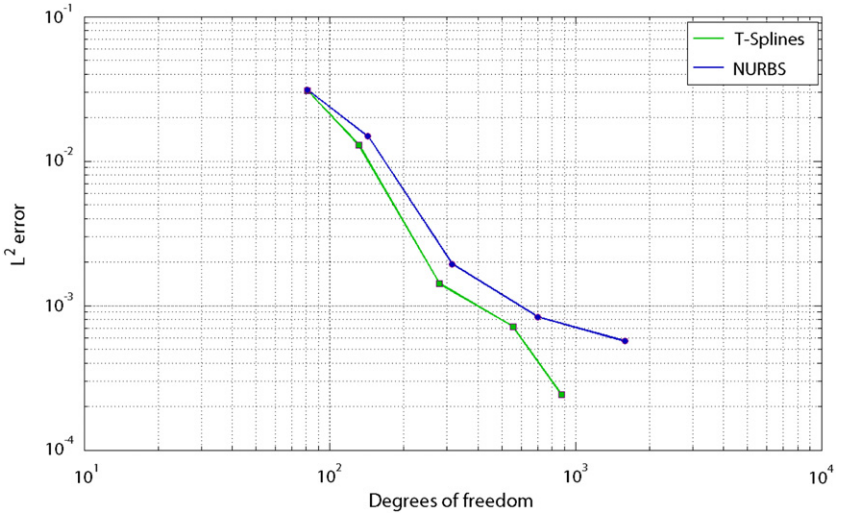

Fig. 6. L^2 velocity error versus degrees of freedom corresponding to the refinement processes depicted in Figs. 4 and 5. The T-spline meshes are locally h-refined based on comparison with the analytic solution. The NURBS results (blue curve) correspond to the unique NURBS refinement of each of the T-spline meshes. (For interpretation of the references to colour in this figure legend, the reader is referred to the web version of this article.)

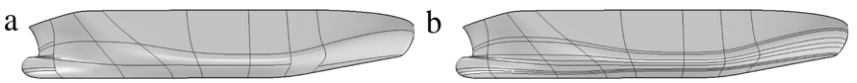

Fig. 7. T-spline (a) and NURBS (b) surface model of the ship hull.

Fig. 6 illustrates that, for a given level of L^2-error, the T-spline based local refinement process requires considerably fewer degrees of freedom compared to the corresponding NURBS-based global refinement process (e.g., for an error of 5.5×10^{-4} the required degrees of freedom are approximately 600 for the T-spline vs. 1600 for the corresponding NURBS representation, i.e., a reduction of 62.5%).

5.2. *Experimenting with a ship hull*

In this example we consider a surface piercing ship moving with constant speed $\mathbf{U} = (U, 0, 0)$. The T-spline surface model of the ship hull has been constructed within the Rhinoceros modeling system[1] and more specifically by using its T-spline plugin.[2] The resulting T-spline surface, see Fig. 7(a), is locally of polynomial degree three in both directions, has 79 control points and is exported to plug-in's IGA format which guarantees analysis-suitability. Since all interior control points are either T-junctions or have a valence of four, no extraordinary control points exist in the T-mesh thus allowing a unique conversion of the T-spline representation into a single NURBS patch which comprises 132 control points; see Fig. 7(b).

In order to drive a local refinement process and check the corresponding convergence rate of the solution, we have constructed a "reference solution" of the problem by inserting uniformly nine knots in every knot interval of the original NURBS representation and computing the IGA-BEM approximation of μ for the resulting NURBS surface. The obtained mesh along with the corresponding reference solution are depicted in Fig. 8.

The L^2-error associated with the distribution of the solution field μ on the body surface is defined as follows:

$$\left\| \mu_{\text{ref}} - \mu^r \right\|_{L^2} = \left(\int_S |\mu_{\text{ref}}(\mathbf{P}) - \mu^r(\mathbf{P})|^2 dS(\mathbf{P}) \right)^{\frac{1}{2}} \tag{31}$$

[1] http://www.rhino3d.com.
[2] http://www.tsplines.com.

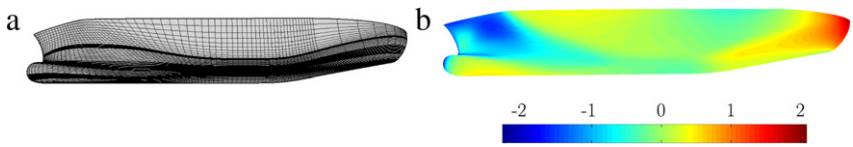

Fig. 8. Uniformly refined NURBS mesh(a) and corresponding reference solution (b).

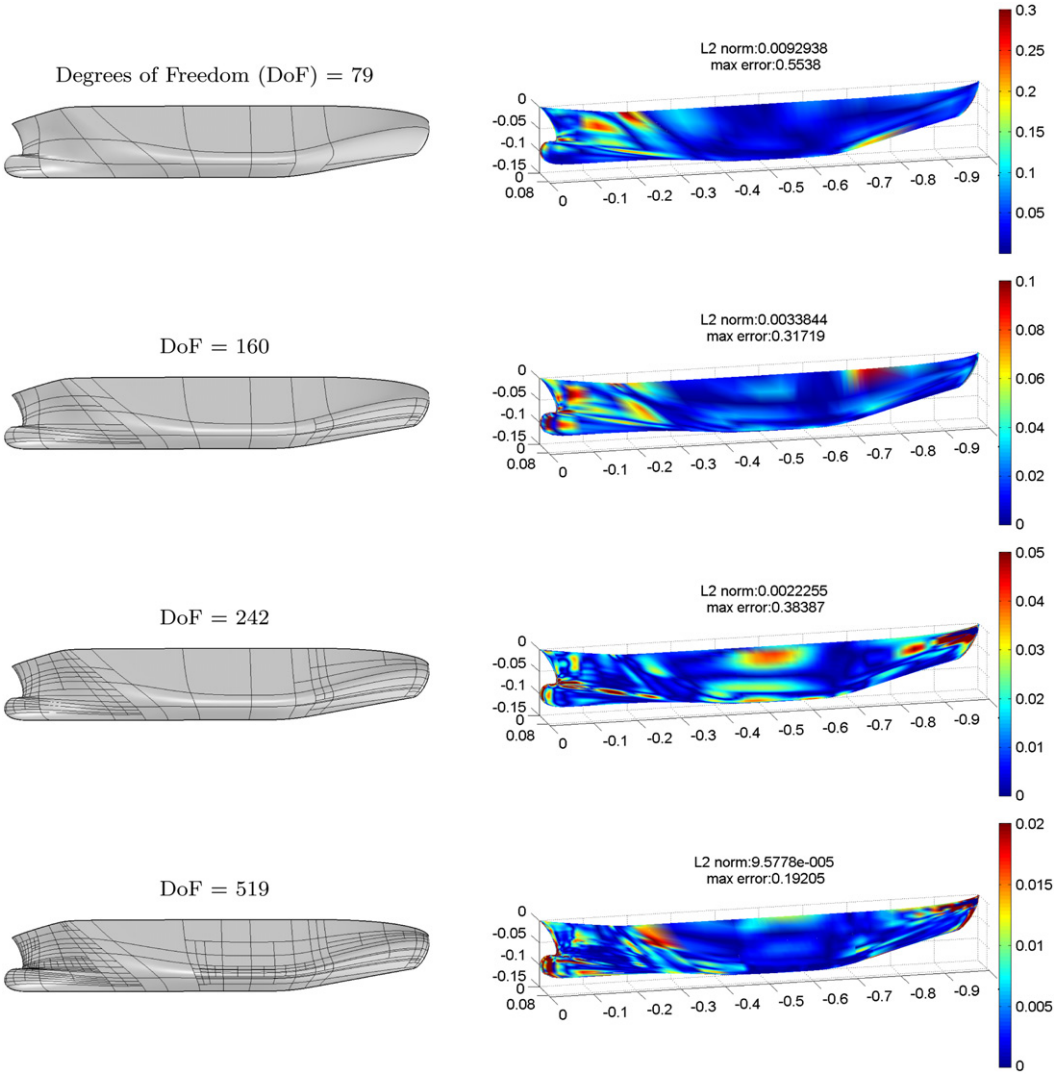

Fig. 9. T-spline refinement steps (left column) along with the corresponding error distribution of the solution μ (right column).

where μ_{ref} denotes the reference solution while μ^r denotes the IGA-BEM approximation of μ corresponding to the refinement level r. The L^2-error associated with the distribution of the pressure coefficient C_p is analogously defined. Fig. 9 depicts the T-mesh of the ship hull along with the corresponding pointwise error $|\mu_{\text{ref}}(\mathbf{P}) - \mu^r(\mathbf{P})|$ of μ for the original mesh and three refinement steps. Each refinement level r is obtained by locally h-refining the T-mesh at level $r-1$ in areas where the error is high. In the first two steps the refinement is confined in the bow and stern areas while the third one involves the middle part as well. The corresponding NURBS based process, where each T-mesh is replaced by its unique NURBS refinement, is given in Fig. 10.

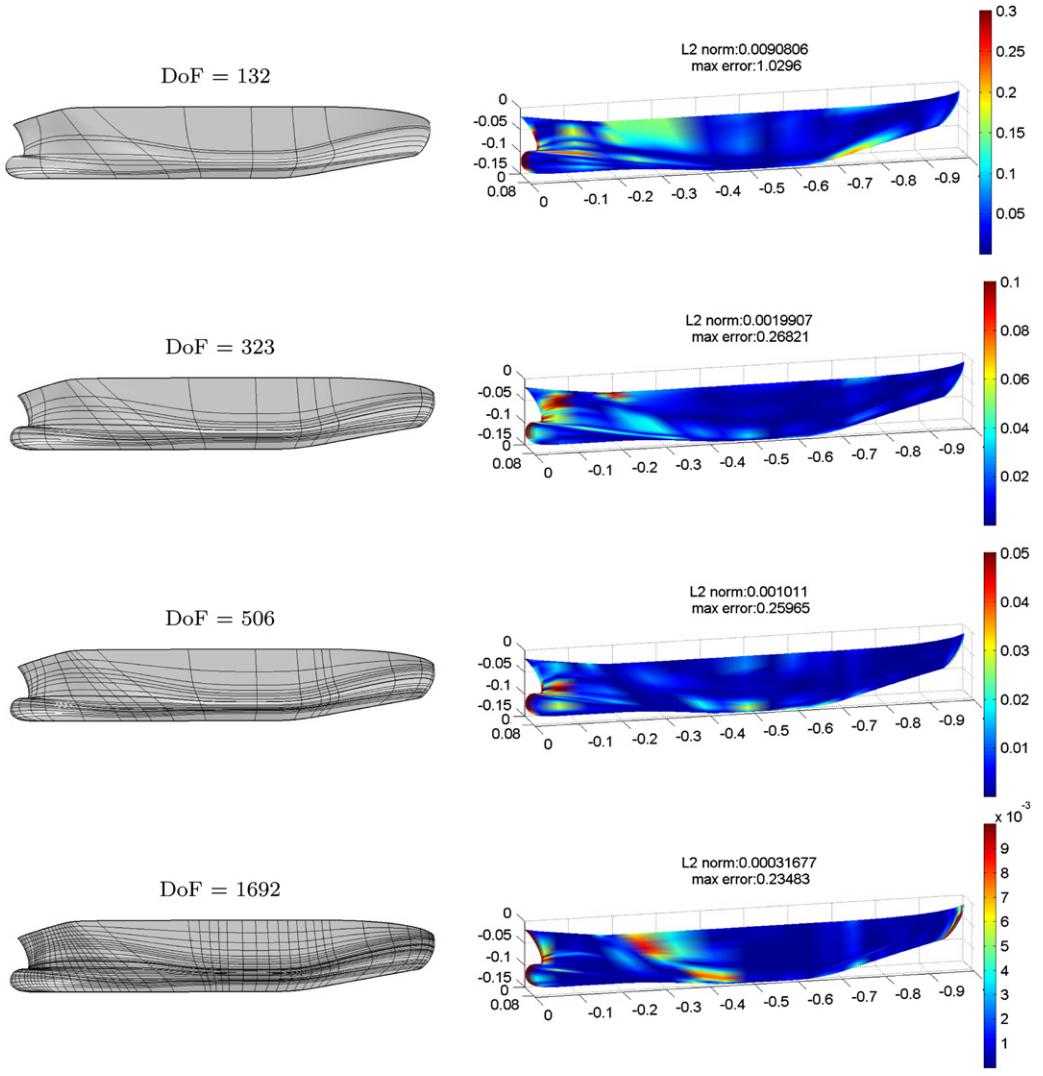

Fig. 10. NURBS refinement steps (left column) along with the corresponding error distribution of the solution μ (right column).

In Fig. 11(a) the L^2-error for μ versus the degrees of freedom is presented for the T-spline based local refinement process (blue curve), the corresponding NURBS refinement (red curve) and the refinement process resulting from inserting uniformly r knots in each parametric interval of the original NURBS representation (green curve). As it can be seen from this figure, for a given error level, the T-spline based refinement requires considerably fewer degrees of freedom as compared to the other two refinement processes. The worst performance occurs, as expected, when using uniform refinement. Analogous remarks can be also made for the L^2-error for C_p, which is presented in Fig. 11(b).

6. Conclusions

In this work, we have demonstrated the advantages of T-splines technology in the context of the ship wave resistance calculation. The higher smoothness of the bases for a single T-spline surface along with the ability for local refinement allowed us to achieve enhanced convergence rates with considerably fewer degrees of freedom when compared to our prior NURBS approach. For the prolate spheroid example, the T-spline based local refinement process requires considerably fewer degrees of freedom compared to the corresponding NURBS-based global refinement process (e.g., for an error of 5.5×10^{-4} the required degrees of freedom are approximately 600 for T-spline vs. 1600

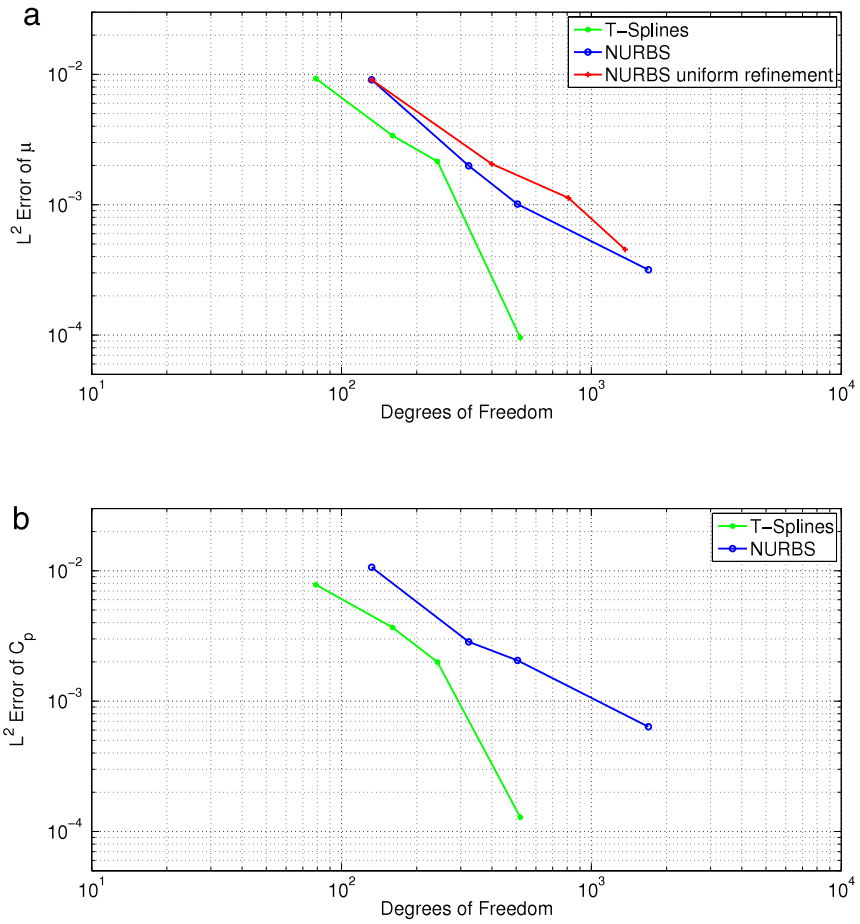

Fig. 11. L^2-error of the density μ (a) and pressure coefficient C_p (b) versus the degrees of freedom corresponding to the refinement processes depicted in Figs. 9 and 10. The T-spline meshes are locally h-refined based on comparison with the reference solution. The NURBS results (blue curve) correspond to the unique NURBS refinement of each of the T-spline meshes. The NURBS uniform refinement (red curve in (a)) extends the coarsest T-spline to its unique NURBS refinement and then uniformly refines it. (For interpretation of the references to colour in this figure legend, the reader is referred to the web version of this article.)

for the corresponding NURBS representation, i.e., a reduction of 62.5%; see Fig. 6). The exact same picture is drawn from our second example, i.e., the ship hull.

This significant enhancement permits our T-spline based IGA-BEM solver to be embedded with significantly lower cost in any optimization process for designing ship hulls with minimum wave resistance; see, e.g. [37]. Future work will focus on this direction as well as on the extension of the methodology to treat effects of nonlinearities in the wave resistance problem.

Acknowledgments

This research has been co-financed by the European Union (European Social Fund — ESF) and Greek national funds through the Operational Program "*Education and Lifelong Learning*" of the National Strategic Reference Framework (NSRF) — Research Funding Program: THALIS-UOA (MIS 375891).

References

[1] J. Michell, The wave resistance of a ship, Phil. Mag. 45 (272).

[2] P.M. Carrica, R.V. Wilson, F. Stern, An unsteady single-phase level set method for viscous free surface flows, Internat. J. Numer. Methods Fluids 53 (2) (2007) 229–256.

[3] L. Larsson, F. Stern, V. Bertram, Benchmarking of computational fluid dynamics for ship flows: the Gothenburg 2000 workshop, Ship Res. 47 (1) (2003) 63–81.
[4] G. Tzabiras, Resistance and self-propulsion calculations for a series 60, cb060 hull at model and full scale, Ship Technol. Res. 51 (2004) 21–34.
[5] I.R. Committee, Report of the resistance committee, in: Proceedings of the 24th International Towing Tank Conference, 2005.
[6] I.R. Committee, Report of the resistance committee, in: Proceedings of the 25th International Towing Tank Conference, 2008.
[7] I.R. Committee, Report of the resistance committee, in: Proceedings of the 26th International Towing Tank Conference, 2011.
[8] T.J.R. Hughes, Isogeometric analysis: progress and challenges, in: International Conference on Mathematical Methods for Curves & Surfaces, MMCS08, Oslo, Norway, 2008.
[9] T.J.R. Hughes, J.A. Cottrell, Y. Bazilevs, Isogeometric analysis: CAD, finite elements, NURBS, exact geometry and mesh refinement, Comput. Methods Appl. Mech. Engrg. 194 (2005) 4135–4195.
[10] J.A. Cottrell, T.J.R. Hughes, Y. Bazilevs, Isogeometric Analysis: Toward Integration of CAD and FEA, Wiley, 2009.
[11] J.A. Cottrell, T.J.R. Hughes, A. Reali, Studies of refinement and continuity in isogeometric structural analysis, Comput. Methods Appl. Mech. Engrg. 196 (2007) 4160–4183.
[12] L. Piegl, W. Tiller, The Nurbs Book, second ed., Springer Verlag, 1997.
[13] C. Politis, A. Ginnis, P. Kaklis, K. Belibassakis, C. Feurer, An isogeometric BEM for exterior potential-flow problems in the plane, in: 2009 SIAM/ACM Joint Conference on Geometric and Physical Modeling, 2009.
[14] K. Belibassakis, T. Gerostathis, K.V. Kostas, C. Politis, P.D. Kaklis, A.I. Ginnis, C. Feurer, A BEM-isogeometric method with application to the wavemaking resistance problem of ships at constant speed, in: 30th International Conference on Offshore Mechanics and Arctic Engineering, 2011.
[15] K.A. Belibassakis, T.P. Gerosthathis, K.V. Kostas, C.G. Politis, P.D. Kaklis, A.-A. Ginnis, C. Feurer, A BEM-Isogeometric method for the ship wave-resistance problem, Ocean Eng. 60 (2013) 53–67.
[16] R. Simpson, S. Bordas, J. Trevelyan, T. Rabczuk, A two-dimensional isogeometric boundary element method for elastostatic analysis, Comput. Methods Appl. Mech. Engrg. 209–212 (0) (2012) 87–100. http://dx.doi.org/10.1016/j.cma.2011.08.008. URL http://www.sciencedirect.com/science/article/pii/S0045782511002635.
[17] K. Li, X. Qian, Isogeometric analysis and shape optimization via boundary integral, Comput. Aided Des. 43 (11) (2011) 1427–1437.
[18] M.A. Scott, R.N. Simpson, J.A. Evans, S. Lipton, S.P.A. Bordas, T.J.R. Hughes, T. Sederberg, Isogeometric boundary element analysis using unstructured T-splines, Comput. Methods Appl. Mech. Engrg. 254 (0) (2013) 197–221. http://dx.doi.org/10.1016/j.cma.2012.11.001. URL http://www.sciencedirect.com/science/article/pii/S0045782512003386.
[19] R.N. Simpson, M.A. Scott, M. Taus, D.C. Thomas, H. Lian, Acoustic isogeometric boundary element analysis, Comput. Methods Appl. Mech. Engrg. 269 (2014) 265–290.
[20] R. Brard, The representation of a given ship form by singularity distributions when the boundary condition on the free surface is linearized, Ship Res. 16 (1972) 79–82.
[21] J.J.M. Baar, W.G. Price, Developments in the calculation of the wavemaking resistance of ships, Proc. R. Soc. Lond. Ser. A Math. Phys. Sci. 462 (1988) 115–147.
[22] KRISO, KRISO Container Ship (KCS), 1997. www.nmri.go.jp/institutes/fluid_performance_evaluation/cfd_rd/cfdws05/Detail/KCS/kcs_l&r.htm.
[23] R. Sharma, T.-W. Kim, R. Lee Storch, H.J. Hopman, S.O. Erikstad, Challenges in computer applications for ship and floating structure design and analysis, Comput. Aided Des. 44 (2012) 166–185.
[24] H.J. Koelman, A mid-term outlook on computer aided ship design, in: COMPIT'13 Proceedings of the 12th International Conference on Computer Applications and Information Technology in the Maritime Industries, Ancona, Italy, 2013, pp. 110–119.
[25] D. Forsey, R. Bartels, Hierarchical B-spline refinement, SIGGRAPH Computer Graphics 22 (4) (1988) 205–212.
[26] T.W. Sederberg, J. Zheng, A. Bakenov, A. Nasri, T-splines and TNURCCs, ACM Trans. Graph. 22 (2003) 477–484.
[27] Y. Bazilevs, V.M. Calo, J.A. Cottrell, J.A. Evans, T.J.R. Hughes, S. Lipton, M.A. Scott, T.W. Sederberg, Isogeometric analysis using T-splines, Comput. Methods Appl. Mech. Engrg. 199 (5–8) (2010) 229–263.
[28] J. Deng, F. Chen, X. Li, C. Hu, W. Tong, Z. Yang, Y. Feng, Polynomial splines over hierarchical t-meshes, GraphicalModels 70 (4) (2008) 76–86.
[29] T. Dokken, T. Lyche, K. Pettersen, Polynomial splines over locally refined box-partitions, Comput. Aided Geom. Design 30 (3) (2013) 331–356.
[30] T.W. Sederberg, J. Zheng, X. Song, Knot intervals and multi-degree splines, Comput. Aided Geom. Design 20 (2003) 455–468.
[31] T.W. Sederberg, D.L. Cardon, G.T. Finnigan, N.S. North, J. Zheng, T. Lyche, T-spline simplification and local refinement, ACM Trans. Graph. 23 (2004) 276–283.
[32] M.A. Scott, M.J. Borden, C.V. Verhoosel, T.W. Sederberg, T.J.R. Hughes, Isogeometric finite element data structures based on Bézier extraction of T-splines, Internat. J. Numer. Methods Engrg. 88 (2) (2011) 126–156.
[33] M. Scott, X. Li, T. Sederberg, T. Hughes, Local refinement of analysis-suitable T-splines, Comput. Methods Appl. Mech. Engrg. 213–216 (2012) 206–222. http://dx.doi.org/10.1016/j.cma.2011.11.022. URL http://www.sciencedirect.com/science/article/pii/S0045782511003689.
[34] M.J. Borden, M.A. Scott, J.A. Evans, T.J.R. Hughes, Isogeometric finite element data structures based on Bezier extraction of NURBS, Internat. J. Numer. Methods Engrg. 87 (2011) 15–47.
[35] H. Lamb, Hydrodynamics, sixth ed., Cambridge Univ. Press, 1932.
[36] L. Milne-Thomson, Theoretical Hydrodynamics, fifth ed., McMillan, 1974.
[37] A.I. Ginnis, R. Dunigneau, C. Politis, K.V. Kostas, K. Belibbassakis, T. Gerostathis, P.D. Kaklis, A multi-objective optimization environment for ship-hull design based on a BEM-isogeometric solver, in: The Fifth Conference on Computational Methods in Marine Engineering, Springer, (Marine 2013), Hamburg, Germany, on 29–31 May 2013, 2013.